A Single Oxidosqualene Cyclase Produces the *Seco*-Triterpenoid α-Onocerin[1][OPEN]

Aldo Almeida,[a] Lemeng Dong,[a] Bekzod Khakimov,[b] Jean-Etienne Bassard,[a] Tessa Moses,[c,d] Frederic Lota,[e] Alain Goossens,[c,d] Giovanni Appendino,[f] and Søren Bak[a,2]

[a]Department of Plant and Environmental Science, University of Copenhagen, DK-1871 Frederiksberg C, Denmark
[b]Department of Food Science, University of Copenhagen, DK-1958 Frederiksberg C, Denmark
[c]Ghent University, Department of Plant Biotechnology and Bioinformatics, 9052 Ghent, Belgium
[d]VIB Center for Plant Systems Biology, 9052 Ghent, Belgium
[e]Alkion Biopharma SAS, 91000 Evry, France
[f]Dipartimento di Scienze del Farmaco, Università del Piemonte Orientale, Largo Donegani 2, 28100 Novara, Italy

ORCID IDs: 0000-0001-5284-8992 (A.A.); 0000-0002-1435-1907 (L.D.); 0000-0001-9366-4727 (T.M.); 0000-0002-9330-5289 (F.L.); 0000-0002-1599-551X (A.G.); 0000-0003-4100-115X (S.B.).

8,14-*seco*-Triterpenoids are characterized by their unusual open C-ring. Their distribution in nature is rare and scattered in taxonomically unrelated plants. The 8,14-*seco*-triterpenoid α-onocerin is only known from the evolutionarily distant clubmoss genus *Lycopodium* and the leguminous genus *Ononis*, which makes the biosynthesis of this *seco*-triterpenoid intriguing from an evolutionary standpoint. In our experiments with *Ononis spinosa*, α-onocerin was detected only in the roots. Through transcriptome analysis of the roots, an oxidosqualene cyclase, OsONS1, was identified that produces α-onocerin from squalene-2,3;22,23-dioxide when transiently expressed in *Nicotiana bethamiana*. In contrast, in *Lycopodium clavatum*, two sequential cyclases, LcLCC and LcLCD, are required to produce α-onocerin in the *N. benthamiana* transient expression system. Expression of *OsONS1* in the lanosterol synthase knockout yeast strain GIL77, which accumulates squalene-2,3;22,23-dioxide, verified the α-onocerin production. A phylogenetic analysis predicts that OsONS1 branches off from specific lupeol synthases and does not group with the known *L. clavatum* α-onocerin cyclases. Both the biochemical and phylogenetic analyses of OsONS1 suggest convergent evolution of the α-onocerin pathways. When *OsONS1* was coexpressed in *N. benthamiana* leaves with either of the two *O. spinosa* squalene epoxidases, *OsSQE1* or *OsSQE2*, α-onocerin production was boosted, most likely because the epoxidases produce higher amounts of squalene-2,3;22,23-dioxide. Fluorescence lifetime imaging microscopy analysis demonstrated specific protein-protein interactions between OsONS1 and both *O. spinosa* squalene epoxidases. Coexpression of *OsONS1* with the two *OsSQE*s suggests that OsSQE2 is the preferred partner of OsONS1 in planta. Our results provide an example of the convergent evolution of plant specialized metabolism.

Triterpenoids are a class of isoprenoids characterized by an amazing structural diversity. Triterpenoids are derived mainly from the 30-carbon precursor squalene-2,3-oxide (SQO), which is synthesized from squalene by squalene epoxidases (SQEs). The next step in triterpenoid biosynthesis is the cyclization of SQO mediated by oxidosqualene cyclases (OSCs; Augustin et al., 2011). Cyclization initiates with the acid-catalyzed epoxide ring opening of SQO and continues through a series of methyl and hydride shifts (Abe, 2014) that give a series of conformationally discrete carbocation intermediates (Van Tamelen et al., 1982; Boar et al., 1984). Carbocation shifting in the catalytic cavity of the OSC is a dynamic process (Tian and Eriksson, 2012) that terminates by deprotonation of the carbocation intermediate, resulting in the formation of a neutral compound. Some OSCs deprotonate a single carbocation intermediate and, thus, form a single cyclized product, while others have the plasticity to deprotonate several carbocations at different positions, rendering them multifunctional and capable of releasing multiple cyclized products (Lodeiro et al., 2007; Wu et al., 2008). Thus, OSCs increase triterpenoid diversity by producing distinct triterpenoid skeletons, with over 100 triterpenoid

[1] The research leading to these results has received funding to TriForC from the European Community's Seventh Framework Programme [FP7/2007-2013] under grant agreement 613692. T.M. was supported by the Special Research Funds from Ghent University.

[2] Address correspondence to bak@plen.ku.dk.

The author responsible for distribution of materials integral to the findings presented in this article in accordance with the policy described in the Instructions for Authors (www.plantphysiol.org) is: Søren Bak (bak@plen.ku.dk).

A.A., S.B., and G.A. conceived the original research plan; A.A. performed most of the experiments, analyzed the data, and drafted the article; J.-E.B. assisted in the design and performance of FLIM experiments; B.K. provided the GC-MS analysis; T.M. and A.G. were involved in the yeast expression experiments; F.L. generated the hairy root lines; L.D. and S.B. supervised and, together with A.A., complemented the writing.

[OPEN] Articles can be viewed without a subscription.
www.plantphysiol.org/cgi/doi/10.1104/pp.17.01369

skeletons estimated to originate from their action (Xu et al., 2004).

The *seco*-triterpenoids are characterized by the presence of an open ring, a structural element that can be connected directly to the cyclization mechanism or result from postcyclization bond cleavage. In this study, we focused on the *seco*-triterpenoid α-onocerin (Fig. 1), a symmetrical tetracyclic triterpenoid first isolated in 1855 from *Ononis spinosa* (Hlasiwetz, 1855) but only structurally elucidated a century later by Barton and Overton (1955). More than a decade after this work, α-onocerin was isolated from the club moss *Lycopodium clavatum* (Ageta et al., 1962) as well.

The occurrence of α-onocerin in only two phylogenetically distant branches of the plant kingdom makes the biosynthesis of α-onocerin intriguing from an evolutionary standpoint. In fact, the occurrence of α-onocerin is inconsistent even within the *Ononis* genus. In a survey of α-onocerin accumulation in *Ononis* spp., extracts from three species were recorded as lacking α-onocerin: *Ononis reclinata*, *Ononis viscosa*, and *Ononis pusilla* (Rowan and Dean, 1972). Decades later, *Ononis rotundifolia* was reported as another non-α-onocerin producer (Hayes, 2012). The *Ononis* genus is monophyletic and splits into five major clades (Turini et al., 2010); however, there is no clear clustering of α-onocerin-producing species, as the nonproducing species are found in the four major clades that have been tested for α-onocerin accumulation. The simultaneous occurrence of α-onocerin-producing and nonproducing species in a couple of monophyletic subsections of the genus, such as *Ononis pubescens* and *O. viscosa* of the Viscosae and *Ononis minutissima* and *O. pusilla* in the Bugranoides, suggests that the ancestral species of the *Ononis* genus gained the trait to produce α-onocerin and that this trait was later lost in some of the *Ononis* spp. during the course of evolution. The biological function of α-onocerin in *Ononis* spp. is unknown; however, it is noteworthy that no natural mutant unable to produce α-onocerin has been reported for *Ononis spinosa*, implying a strong positive selection for retaining this trait in at least this species.

Assays with *O. spinosa* enzyme extracts have shown that α-onocerin is cyclized exclusively from squalene-2,3;22,23-dioxide (SDO) and not the general triterpenoid precursor SQO (Rowan et al., 1971). Accordingly, two key steps for α-onocerin biosynthesis are anticipated. First, an efficient SQE has to provide the cyclase(s) with sufficient amounts of SDO under regular physiological conditions. SQEs from different organisms ranging from mammals (Bai et al., 1992) to plants (Rasbery et al., 2007) have been reported to produce SDO, although only when the subsequent cyclization steps were chemically inhibited for a couple of hours with 2-isopropyl-4-dimethylamino-5-methylphenyl-1-piperdiner carboxylate methyl chloride (AMO-1618) or 3β-(β-dimethylaminoethoxy)-androst-5-en-17-one (DMAE-DHA). This inhibition allows the accumulation of SQO and its further conversion to SDO (Field and Holmlund, 1977; Nagumo et al., 1995). The second interesting step in α-onocerin biosynthesis is the cyclization reaction. Recently, it was shown that, in *L. clavatum*, the biosynthesis of α-onocerin is performed in two steps by two substrate-specific OSCs acting sequentially. LcLCC cyclizes SDO to the two-ring structure pre-α-onocerin, after which LcLCD initiates cyclization from the remaining epoxide bond of pre-α-onocerin to finally produce α-onocerin (Araki et al., 2016). However *L. clavatum* and *O. spinosa* are phylogenetically very distant, with the former being a lycopod and the latter an angiosperm. Therefore, it is likely that the α-onocerin pathways evolved convergently in these two plant species.

Another aspect of triterpenoid biosynthesis that has been overlooked in the literature is the uptake of SQE products by OSCs. It has been suggested that the sterol pathway proceeds by the channeling of substrates between each step through microdomains of the endoplasmic reticulum (ER; Benveniste, 2004). However, it is known that active SQE and OSC enzymes can localize to related but nevertheless distinct cell compartments (e.g. in yeast, active SQE is found on/in the ER, whereas active lanosterol synthase is found in lipid droplets along with the inactive form of SQE; Leber et al., 1998; Athenstaedt et al., 1999). Aside from the probable close proximity of lipid droplets to the ER membrane network, another force driving triterpenoid biosynthesis could be protein-protein interactions. Surprisingly, protein-protein interactions between SQEs and OSCs have not been reported, in spite of existing evidence of specific SQE homologs coexpressing with different enzymes of specialized metabolism, specifically OSCs (Suzuki et al., 2002).

In this study, we identify and characterize a single OSC from *O. spinosa* that can produce α-onocerin as well as two SQEs that can boost α-onocerin production upon transient expression in *Nicotiana benthamiana*. In addition, we report protein-protein interactions of the α-onocerin synthase from *O. spinosa* with the SQEs from the same species. Insights into the spatiotemporal contrasts of α-onocerin accumulation and α-onocerin biosynthesis in the roots of *O. spinosa* also are provided.

RESULTS

Wild *O. spinosa* Accessions Accumulate α-Onocerin in the Roots

To identify plant material suitable for gene discovery in the α-onocerin biosynthetic pathway, accessions of *Ononis* spp. were collected from several sources and screened for their α-onocerin content (Table I). All *O. spinosa* accessions analyzed contained α-onocerin in the roots but not in aerial tissues, as indicated by thin-layer chromatography (TLC) and gas chromatography-mass spectrometry (GC-MS) analyses of dichloromethane extracts (Supplemental Fig. S1A). Extracts from the accession Ont03 (*Ononis natrix*) analyzed by TLC showed a spot on the TLC plate that

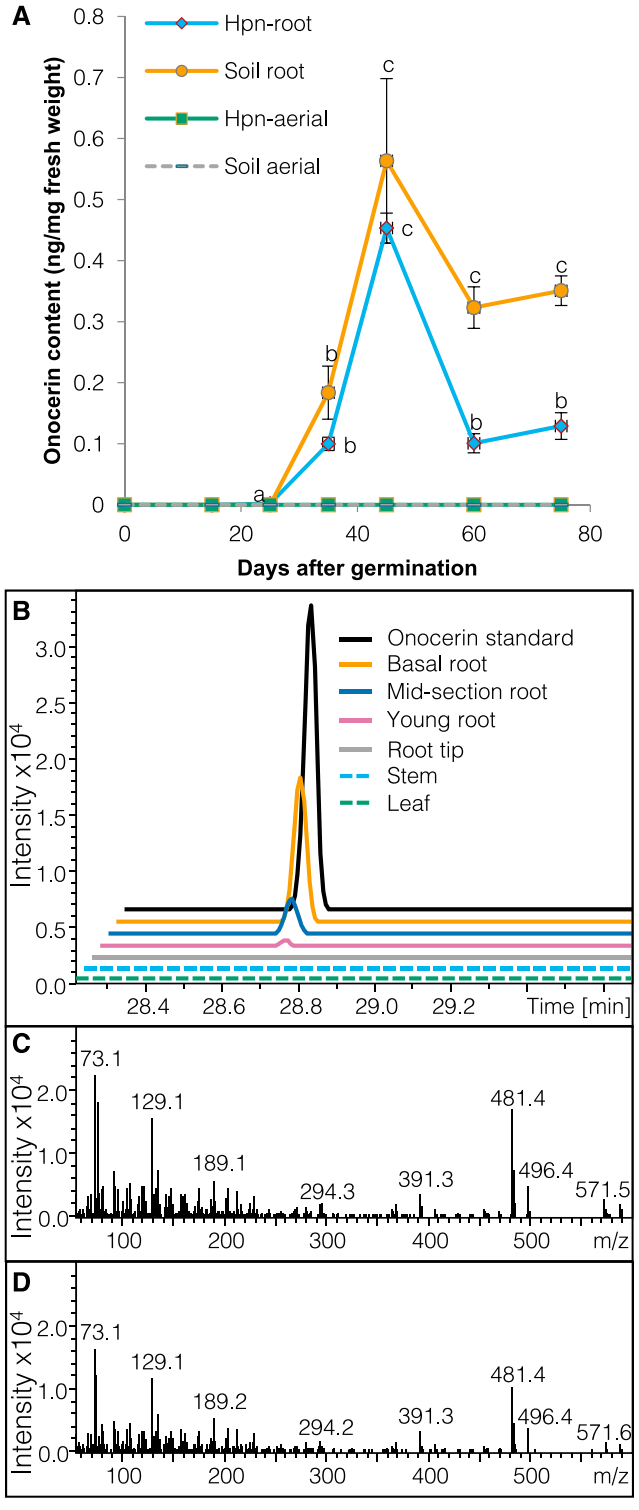

Figure 1. α-Onocerin content varies throughout plant growth and across the root length. A, Time course of α-onocerin accumulation in root and aerial tissues (fresh weight) of *O. spinosa* plants grown in either soil or a hydroponics (Hpn) system. B, Extracted ion chromatograms (480–482 mass-to-charge ratio) of *O. spinosa* root sections, stem, and leaf tissues. C, Mass spectrum of derivatized α-onocerin standard. D, Representative mass spectrum of an α-onocerin peak in derivatized extracts from root sections. Values represent means ± SE from three biological replicates for each time point; letters indicate significant differences determined by ANOVA/posthoc Tukey's honestly significant difference (HSD) test at $P < 0.05$.

comigrated with the α-onocerin standard (Supplemental Fig. S1A); however, GC-MS analysis revealed that it was not α-onocerin (Supplemental Fig. S1B). These data suggest that *O. natrix* should be added to the list of *Ononis* spp. that do not produce α-onocerin, as α-onocerin was not detected in any of the three replicates of the three *O. natrix* accessions tested.

The wild accession OsDK7 was selected for pathway elucidation, as it displayed high α-onocerin content and seeds were readily available. To determine the optimal OsDK7 root material for gene discovery, the accumulation of α-onocerin was monitored across several time points for plants grown hydroponically and in soil (Fig. 1A). In roots of hydroponically grown *O. spinosa* plants, the accumulation of α-onocerin was differentially regulated throughout growth. α-Onocerin could not be detected in the roots during early periods of development (15 d after germination) but could be detected in trace amounts 25 d after germination (0.0019 ± 0.0003 ng mg^{-1} fresh weight). Subsequently, a sharp increase was observed 35 d after germination (0.099 ± 0.018 ng mg^{-1}), with the concentration peaking 45 d after germination (0.45 ± 0.04 ng mg^{-1}). α-Onocerin content dropped 60 d after germination to levels similar to those observed at 35 d and remained in that range 75 d after germination.

The α-Onocerin content of OsDK7 plants grown in soil was similarly monitored throughout growth at several time intervals. Sufficient amounts of root tissue could not be obtained from plants 15 and 25 d after germination and, therefore, were not analyzed. At 35 d after germination, roots contained ~0.18 ± 0.07 ng mg^{-1} α-onocerin, and the accumulation of α-onocerin peaked 45 d after germination (0.56 ± 19 ng mg^{-1}) to levels comparable to those of hydroponically grown plants of the same age.

Finally, *O. spinosa* hairy roots were generated, as it is well know that hairy roots can accumulate elevated levels of plant specialized metabolites and, thus, could present an alternative to the hydroponic and soil-grown roots. To generate stable hairy root lines, OsDK7 leaf tissue was transformed with *Agrobacterium rhizogenes* strain LBA9402 *virGN54D*. Two hairy root lines, designated Ohry1 and Ohry2 (Supplemental Fig. S2, A and B), were obtained that produced α-onocerin. Ohry1 produced ~4 times less α-onocerin than Ohry2 (0.007 ± 0.002 and 0.029 ± 0.004 ng mg^{-1} fresh weight, respectively). Nonetheless, α-onocerin production in Ohry2 cultures was still ~15-fold lower than that in 45-d-old hydroponic roots of OsDK7 (Supplemental Fig. S2C). Consequently, further work was continued with OsDK7 plants grown in the hydroponic system, as they were cleaner and easier to process than those grown in soil and accumulated more α-onocerin than the hairy root lines.

Table I. *Presence of α-onocerin in the* Ononis *spp. accessions sampled*

Label	Species	Serial Number	α-Onocerin		Source/Location
			Roots	Aerial	
OsDK01	*O. spinosa*	Wild	+	−	Mulkholm, Denmark (latitude, 55.674585; longitude, 11.844718)
OsDK02	*O. spinosa*	Wild	+	−	Mulkholm, Denmark (latitude, 55.683618; longitude, 11.829641)
OsDK03	*O. spinosa*	Wild	+	−	Røsnæs, Denmark (latitude, 55.735394; longitude, 10.891202)
OsDK04	*O. spinosa*	Wild	+	−	Røsnæs, Denmark (latitude, 55.733825; longitude, 10.893441)
OsDK05	*O. spinosa*	Wild	+	−	Røsnæs, Denmark (latitude, 55.733014; longitude, 10.894868)
OsDK06	*O. spinosa*	Wild	+	−	Røsnæs, Denmark (latitude, 55.731662; longitude, 10.900188)
OsDK07	*O. spinosa*	Wild	+	−	Nekselø, Denmark (latitude, 55.771877; longitude, 11.293105)
Osp01	*O. spinosa*	16847	+	−	Botanische Gärten der Universität Bonn, Germany
Osp02	*O. spinosa*	N/A	+	−	Sheffield Seed Company, New York, United States
Osp03	*O. spinosa*	N/A	+	−	Jardin des Plantes et Botanique, Caen, France
Ont01	*O. natrix*	199706	−	−	Origin, Madaba, Jordan (maintained by Millennium Seed Bank [MSB], Kew Royal Botanical Gardens, United Kingdom)
Ont02	*O. natrix*	122227	−	−	Origin, Zahle, Lebanon (maintained by MSB, Kew Royal Botanical Gardens, United Kingdom)
Ont03	*O. natrix*	83951	−	−	Origin, Essaouira, Morocco (maintained by MSB, Kew Royal Botanical Gardens, United Kingdom)

α-Onocerin Accumulates Differently in *O. spinosa* Root Sections

To narrow down tissues for transcriptome analysis, we further investigated the accumulation of α-onocerin across the length of *O. spinosa* hydroponically grown roots at 45 d after germination. The roots were cut in sections and analyzed by TLC (Supplemental Fig. S1C) and GC-MS (Fig. 1B). A pronounced difference in α-onocerin accumulation was observed across the root length: with the highest content of α-onocerin detected in the root base, the second highest in the midsection of the root, and only trace amounts detected in the young roots. α-Onocerin was undetectable in the root tips.

α-Onocerin Is Produced by a Lupeol Synthase-Like OSC, and Its Production Is Boosted by OsSQEs

For gene discovery, RNA sequencing was performed on root tips and midsection roots. Midsection roots were chosen over basal roots since α-onocerin pathway genes in midsection roots were expected to be more actively transcribed than in basal roots, where transcription might have diminished or stopped. A total of 16 million reads were assembled using Trinity, returning a transcriptome of 25,433 predicted genes with an N50 of 1,464 bp.

To select SQE candidates, the *O. spinosa* root transcriptome was mined by BLASTN with the two published *Medicago truncatula* SQEs (AJ430609 and AJ430608) as query sequences. Two contigs were retrieved, and comparison of the coding sequences showed that they are 94% and 78% identical at the amino acid level to *M. truncatula* monooxygenase2, respectively. To confirm the sequence of the contigs, RACE was performed on RNA isolated from OsDK7 roots, and two distinct full-length transcripts were retrieved that were 82% identical to each other on the amino acid level. *OsSQE1* (GenBank accession no. KY625494) showed 91% identity with *M. truncatula* monooxygenase1 and *OsSQE2* (GenBank accession no. KY625495) showed 92% identity to *M. truncatula* monooxygenase2 at the amino acid level. A maximum-likelihood phylogenetic tree was constructed from the deduced amino acid sequences of several SQEs (Fig. 2A) and showed that the two SQEs from *O. spinosa* clustered with their respective SQE orthologs in *M. truncatula*, indicative of an SQE duplication before the speciation of *M. truncatula* and *O. spinosa*.

To select OSC candidates, the *O. spinosa* root transcriptome was analyzed by BLASTN using a small subset of OSC sequences with defined product profiles as queries. Four contigs were identified: *OsCAS* (GenBank accession no. KY657238) showed highest identity to *Pisum sativum* cycloartenol synthase (91% identity at the amino acid level), *OsLAS* (GenBank accession no. KY657237) displayed highest identity to Arabidopsis (*Arabidopsis thaliana*) lanosterol synthase (66%), and *OsBAS* (GenBank accession no. KY657236) showed highest identity to *M. truncatula* BAS1 β-amyrin synthase (94%). The last contig showed 78% identity to *Glycyrrhiza glabra* lupeol synthase, GgLUS1. This contig was considered the most interesting candidate for α-onocerin biosynthesis, since lupeol was not detected in roots or leaves of *O. spinosa*. In addition, lupeol synthases of other species have been shown to be multifunctional (i.e. producing diverse products), as is the case for LUP1 and LUP2 from Arabidopsis. RACE was performed on OsDK7 root RNA with gene-specific primers designed from the lupeol synthase-like contig, which facilitated the isolation and assembly of two distinct transcripts, designated *OsONS1* and *OsONS2*. The principal differences between the transcripts were the lengths of their 5′ untranslated region sequences (146 and 29 bp, respectively) and 25 single-nucleotide polymorphisms across the whole transcript.

The predicted open reading frames of the four OSC transcripts were expressed transiently in *N. benthamiana*

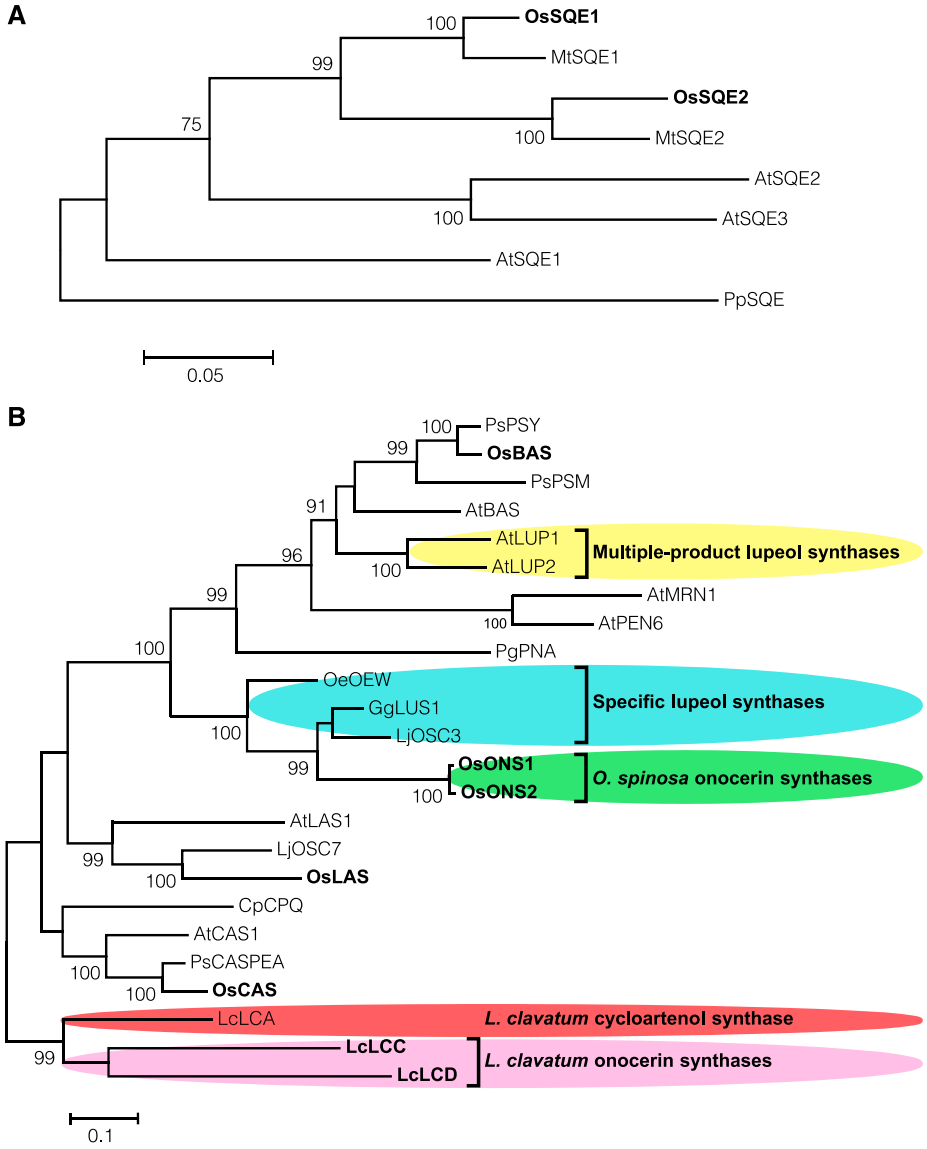

Figure 2. Phylogenetic analysis suggests that the α-onocerin pathway genes in *O. spinosa* and *L. clavatum* are distantly related and arise from convergent evolution. A, Maximum-likelihood tree constructed on deduced amino acid sequences of eight SQEs aligned by ClustalW spanning 496 positions using the MEGA6 program. The statistical significance of each node was tested by the bootstrap method using 1,000 iterations. Representative names are as follows: OsSQE1, *O. spinosa* squalene epoxidase1; MtSQE1, *M. truncatula* mRNA for squalene monooxygenase1; AtSQE1, Arabidopsis squalene epoxidase1; PpSQE, *Physcomitrella patens* squalene epoxidase. B, Maximum-likelihood tree constructed on deduced amino acid sequences of 24 OSCs with known product profiles aligned by ClustalW spanning 730 positions using the MEGA6 program. The statistical significance of each node was tested by the bootstrap method using 1,000 iterations. Boldface names represent genes from *O. spinosa* and *L. clavatum*. Representative names are as follows: OsONS1, *O. spinosa* onocerin synthase1; OsBAS, *O. spinosa* putative β-amyrin synthase; OsCAS, *O. spinosa* putative cycloartenol synthase; OsLAS, *O. spinosa* putative lanosterol synthase; PsCASPEA, *P. sativum* cycloartenol synthase; PsOSCPSY, *P. sativum* β-amyrin synthase; PsOSCPSM, *P. sativum* mixed amyrin synthase; MtBAS, *M. truncatula* β-amyrin synthase; AtLUP1, Arabidopsis lupeol synthase1; AtPEN6, Arabidopsis *seco*-β-amyrin synthase; AtMRN1, Arabidopsis marneral synthase; AtBAS, Arabidopsis β-amyrin synthase; AtCAS1, Arabidopsis cycloartenol synthase; AtLAS1, Arabidopsis lanosterol synthase; PgPNA, *Panax ginseng* dammarenediol II synthase; LcLCA, *L. clavatum* cycloartenol synthase; LcLCC, *L. clavatum* pre-α-onocerin synthase; LcLCD, *L. clavatum* onocerin synthase; OeOEW, *Olea europaea* lupeol synthase; GgLUS1, *G. glabra* lupeol synthase; LjOSC3, *Lotus japonicus* lupeol synthase; LjOSC7, *L. japonicus* lanosterol synthase; CpCPQ, *Cucurbita pepo* cucurbitadienol synthase. GenBank accession numbers for each nucleotide sequence of OSCs and SQEs are given in "Materials and Methods."

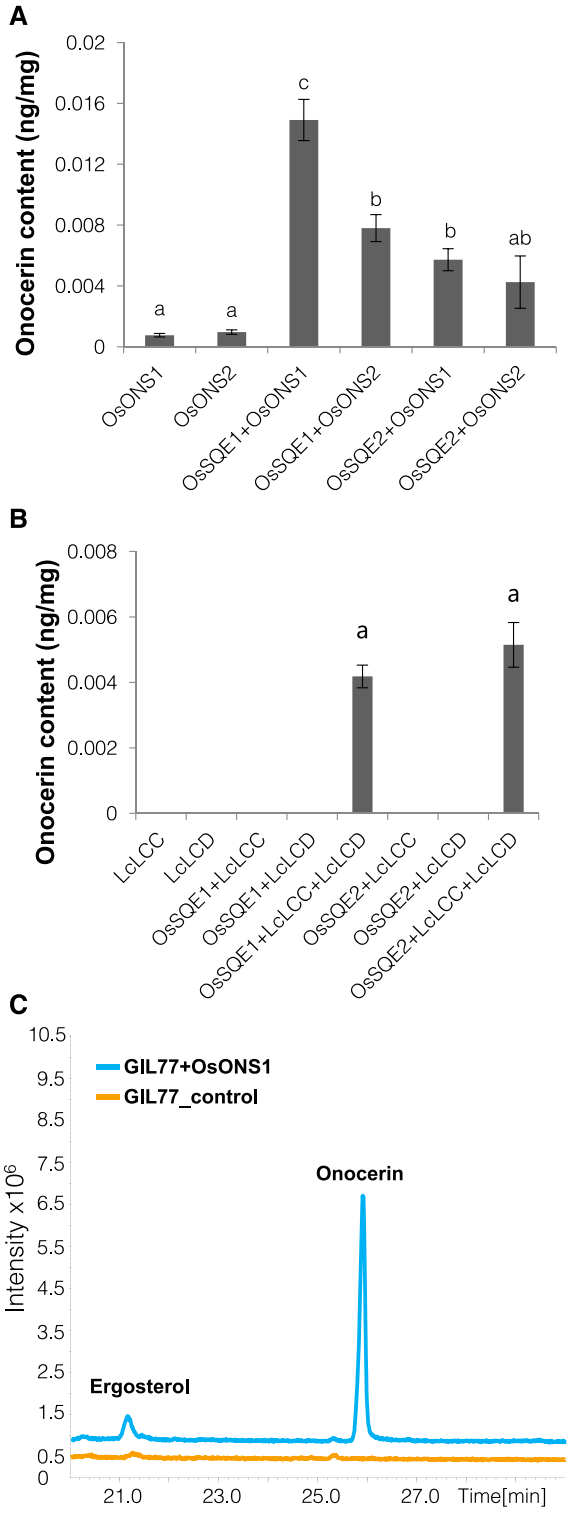

Figure 3. α-Onocerin biosynthesis in *O. spinosa* is biochemically different from that of *L. clavatum*. A, α-Onocerin content of *N. benthamiana* leaves transiently transformed with *OSCs* and *SQEs* of *O. spinosa*. B, α-Onocerin content of *N. benthamiana* leaves transiently transformed with α-onocerin synthases of *L. clavatum* coexpressed with *SQEs* of *O. spinosa*. C, Total ion chromatogram showing the production of α-onocerin in yeast strain GIL77 transformed with *OsONS1* of *O. spinosa*. Values represent means ± SE from three biological replicates; letters indicate significant differences determined by ANOVA/posthoc Tukey's HSD test at $P < 0.05$.

leaves. Five days after infiltration, dichloromethane extracts of the infiltrated leaves were analyzed by GC-MS. α-Onocerin was detected only in leaves expressing *OsONS1* or *OsONS2* (Fig. 3A).

When expressed individually in *N. benthamiana* leaves, both *OsONS1* and *OsONS2* transcripts yielded trace amounts of α-onocerin (0.0007 ± 0.0001 and 0.0009 ± 0.0001 ng mg^{-1} fresh weight, respectively). As α-onocerin has been shown previously to be produced from SDO and not SQO, we speculated that *N. benthamiana* was not supplying enough SDO to the α-onocerin synthases. Therefore, *OsONS1* and *OsONS2* were coexpressed with either *OsSQE1* or *OsSQE2*. Production of α-onocerin by *OsONS1* and *OsONS2* when coexpressed with *OsSQE2* was increased 7.5- and 4.3-fold, respectively (Fig. 3A). However, OsSQE1 increased the production of α-onocerin of OsONS1 by nearly 20-fold. This α-onocerin boost was also ~2.5 times higher than the α-onocerin production boost from the combinations OsONS1+OsSQE2, OsONS2+OsSQE1, and OsONS2+OsSQE2 (Fig. 3A), indicating that the combination of OsSQE1 and OsONS1 is the best performing for α-onocerin biosynthesis.

α-Onocerin Biosynthesis in *O. spinosa* Differs from That in *L. clavatum*

To resolve the phylogenic relationship of the *O. spinosa* OSCs, a maximum-likelihood phylogenetic tree was constructed from a multiple sequence alignment of deduced amino acid sequences of a subset of OSCs with confirmed product profiles (Fig. 2B). The phylogenetic tree showed that LcLCC and LcLCD from *L. clavatum*, known to be involved in the production of α-onocerin in this species, stem from sterol metabolism, being closely related to *L. clavatum* cycloartenol synthase (LcLCA; 58% and 55% identity at amino acid level, respectively). On the other hand, OsONS1 and OsONS2 from *O. spinosa* branch from angiosperm-specialized metabolism from a predisposition to lupeol synthesis of the Fabaceae family and are distantly related to LcLCC and LcLCD.

The *N. benthamiana* transient expression platform was used to compare differences in the α-onocerin biosynthetic pathways of *O. spinosa* and *L. clavatum*. α-Onocerin was not detected when *LcLCC* or *LcLCD* was expressed alone or in combination with *OsSQE1* or *OsSQE2* (Fig. 3B). α-Onocerin accumulation was detected only when *LcLCC* and *LcLCD* were coexpressed together in the presence of either *OsSQE1* or *OsSQE2*. The amount of α-onocerin detected from the *L. clavatum* pathway enzymes was 3 times less than that of the *OsONS1* and *OsSQE1* combination.

To verify the results obtained in *N. benthamiana*, *OsONS1* was expressed in the *erg7* knockout yeast

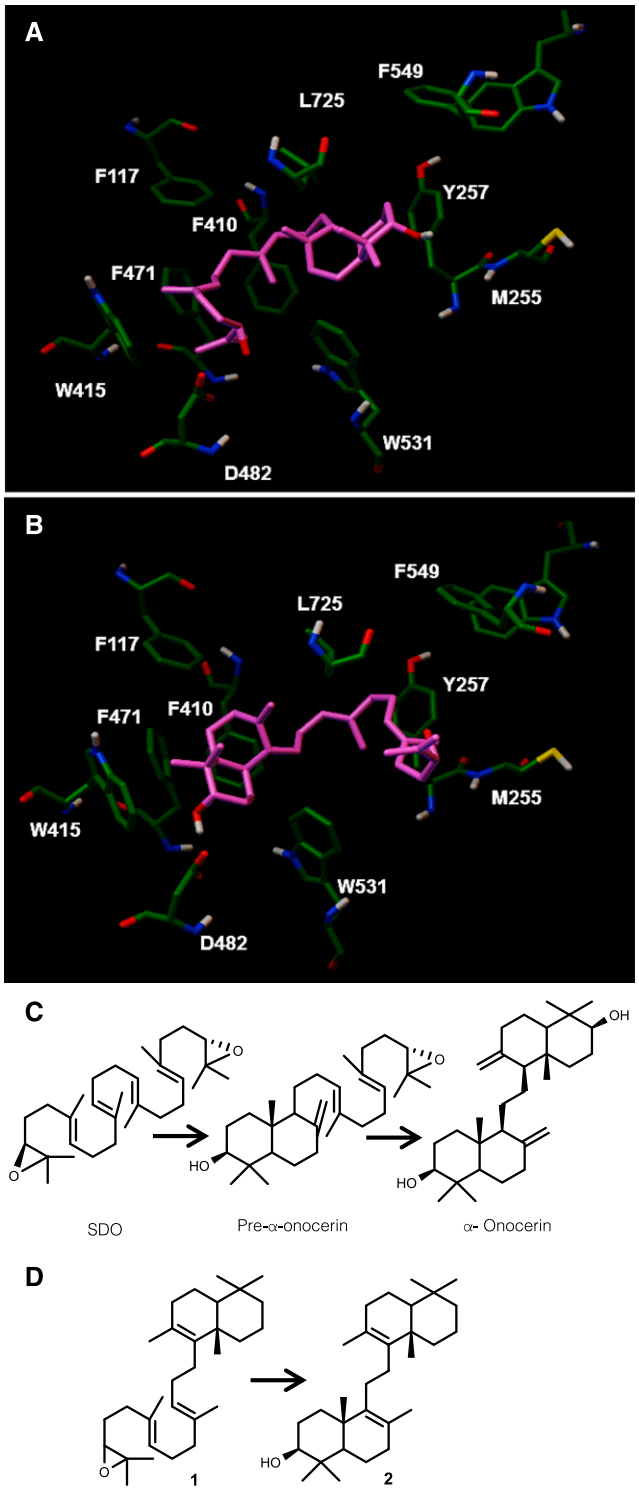

Figure 4. Docking simulations of the OsONS1 homology model shows that pre-α-onocerin can dock from both ends to the catalytic Asp residue, Asp-482. Color coding is as follows: pink, carbon atoms of pre-α-onocerin; green, carbon atoms in amino acid residues of the OsONS1 homology model; red, oxygen atoms; blue, nitrogen atoms; white, hydrogen atoms; yellow, sulfur atoms. A, Epoxide end of pre-α-onocerin forming a hydrogen bond with catalytic Asp-482 in the active site of the OsONS1 homology model. B, Hydroxyl group from the cyclized end of pre-α-onocerin forming a hydrogen bond with catalytic Asp-482 in the active site of the OsONS1 homology model. C, Steps of the α-onocerin biosynthetic pathway. D, Demonstrated cyclization reaction by rabbit microsomes. Compound **1,** 3-((3*E*,7*E*)-3,7-Dimethyl-10-((8a*S*)-2,5,5,8a-tetramethyl-3,4,4a,5,6,7,8,8a-octahydronaphthalen-1-yl)deca-3,7-dien-1-yl)-2,2-dimethyloxirane; compound **2**, 8,14-*seco*-gammacera-7,14-diene-3-ol.

strain GIL77. This strain is known to accumulate high amounts of SDO and does not express other OSCs, ensuring that the triterpenoids isolated from the cultures are synthesized solely by the heterologously expressed OSC. GIL77 cultures expressing *OsONS1* produced α-onocerin (Fig. 3C), confirming that α-onocerin was biosynthesized by the single cyclase.

The biosynthesis of α-onocerin in *L. clavatum* has been shown to require two sequential steps catalyzed by LcLCC and LcLCD. LcLCC first cyclizes SDO to pre-α-onocerin, which is cyclized subsequently by LcLCD to α-onocerin, starting the cyclization from the remaining epoxide end (Fig. 4). To evaluate how OsONS1 synthesizes α-onocerin, in silico molecular docking simulations were performed. These models aim to establish if OsONS1 can perform the two sequential steps known for *L. clavatum* OSCs or if it can cyclize both ends of SDO simultaneously in the active site. A homology model of OsONS1 was constructed based on the crystal structure of human lanosterol synthase (HsLAS). The model was evaluated using the Prosaweb server and checked for Ramachandra outliers through the Molprobity server. Correct modeling of the active site was inspected manually. First, the multiple sequence alignment showed no indication that the active site could protonate both ends of SDO simultaneously, since there was no second DCTAE motif (or a similar one). The DCTAE motif is conserved in all OSCs and is responsible for the protonation of the epoxide ring that begins the cyclization cascade. Absence of a second catalytic motif facing the regular DCTAE motif was confirmed by the homology model (Fig. 4, A and B). An alternative for simultaneous cyclization would be if OsONS1 forms a homodimer with the active sites in close proximity facing one another and both ends of SDO are cyclized simultaneously. However, this last hypothesis is unlikely for two reasons. First, the size of SDO in a prefolded conformation is estimated to be ~6 Å, which is too small to span two active sites. Second, the OSCs follow a strict mechanism by which the substrate enters the active site through a substrate channel. Therefore, it is more likely that OsONS1 is promiscuous for both SDO and pre-α-onocerin. Molecular docking simulations run for pre-α-onocerin revealed that the molecule could be docked in the active site, interacting with the catalytic residue Asp-482 in the OsONS1 protein model at both the cyclized and epoxide ends (Fig. 4, A and B). The binding energy for the residue Asp-482 forming a hydrogen bond with the hydroxyl group

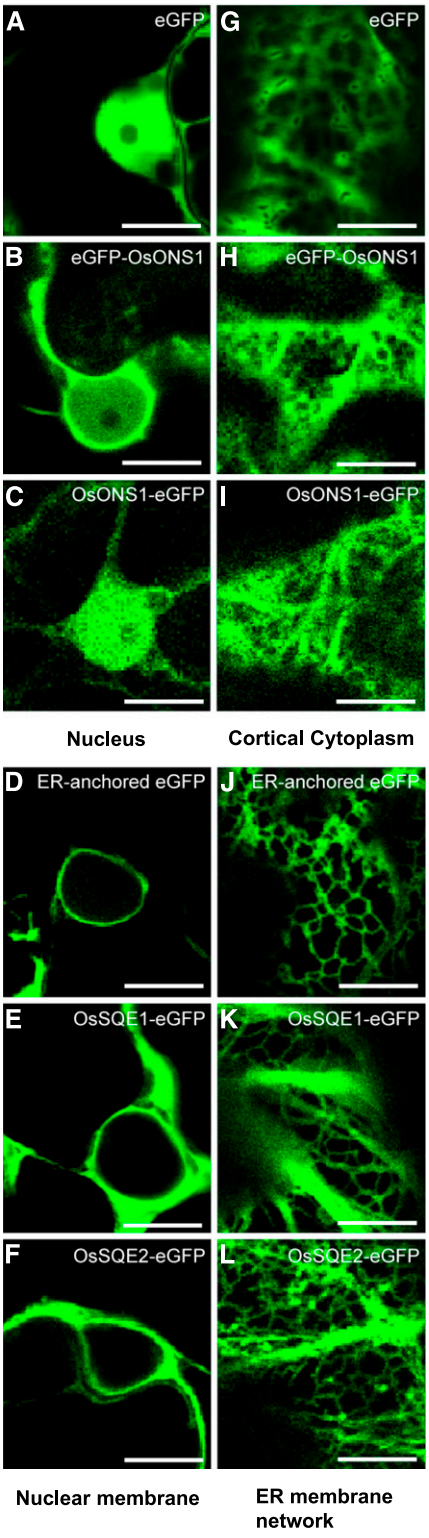

Figure 5. OsONS1 localizes in the cytoplasm while OsSQEs are restricted to the ER membrane, as visualized by confocal microscopy of *N. benthamiana* epidermal leaves. Confocal laser scanning microscopy images were collected 3 d after agroinfiltration of *N. benthamiana* leaves. Representative confocal images of the nucleus (A–F) and parietal cell space (G–L) of leaves expressing eGFP-tagged target proteins are shown. Soluble enzymes may permeate through the nuclear pores and be found inside the nucleus (A–C) and fill out the cytoplasm around the cortical ER (G–I). ER proteins are restrained to nuclear membranes (D–F) and to a characteristic ER membrane network (J–L). Due to turgescent vacuole pushing the cytoplasm and ER near the plasma membrane, a well-defined ER network and diffused cytoplasmic patterns may be visualized when observing the cortical space in epidermal cells of *N. benthamiana* leaves. Bars = 10 μm.

of pre-α-onocerin was -11.84 kcal mol^{-1} (Fig. 4A), whereas that of Asp-482 interacting with the epoxide end of pre-α-onocerin was -2.32 kcal mol^{-1} (Fig. 4B). This supported the hypothesis that OsONS1 cyclizes SDO to pre-α-onocerin, which is later diffused out of the active site and then reenters to be cyclized into α-onocerin.

OsONS1 and OsSQEs Localize to Neighboring Subcellular Compartments and Show Protein-Protein Interactions

In the *N. benthamiana* coexpression experiments, OsSQE1 boosted α-onocerin production 2.6-fold more than OsSQE2. To determine if α-onocerin production was boosted due to the overproduction of SDO by OsSQE1, or if it was due to protein-protein interaction of OsONS1 with OsSQE1, leading to metabolic channeling, different combinations of N- and C-terminally fluorescently tagged OsONS1 and OsSQEs were coexpressed and analyzed using fluorescence lifetime imaging microscopy (FLIM).

FLIM is a fluorescence/Förster resonance energy transfer (FRET)-based method to investigate protein-protein interactions, in which measurements are dependent on the fluorophore concentrations. Therefore, for an optimal protein-protein interaction assay, it is generally advised that the least expressed partner is fused to the FRET donor (eGFP tag) and the most expressed partner to the FRET acceptor (mRFP1 tag; Lalonde et al., 2008). Accordingly, constructs of *OsONS1*, *OsSQE1*, and *OsSQE2* fused to *eGFP* at either the N or C terminus were prepared. This enabled a qualitative assessment of the expression of the constructs in *N. benthamiana* and additionally revealed the subcellular localization of the enzymes.

Confocal images of OsONS1 constructs tagged at both C and N termini showed OsONS1 to be soluble and localized in the cytoplasm, filling the space around the cortical ER (Fig. 5, G–I) as well as entering the nucleus (Fig. 5, A–C). The addition of the tag at either the N or C terminus did not influence the observed localization of OsONS1. In contrast, both OsSQE1 and OsSQE2 tagged at the C terminus were localized exclusively to the ER network membranes (Fig. 5, J–L) and nuclear membrane (Fig. 5, D–F). However, when OsSQEs were tagged with eGFP at the N terminus, no fluorescence was detectable, suggesting that the tag at the N terminus interfered with the expression, stability, or localization of the protein.

Hence, C-terminally tagged SQEs were used for further FLIM measurements.

Overall, confocal imaging revealed that OsSQEs C-terminally tagged with eGFP displayed higher brightness compared with that observed for OsONS1 tagged at either the C or N terminus, indicating that *OsSQE* constructs were expressed higher relative to *OsONS1* constructs. Therefore, constructs of *OsONS1* fused to eGFP at either the C or N terminus were chosen as the energy donors and *OsSQEs* were fused to mRFP1 at the C terminus and used as the energy acceptors in subsequent FLIM experiments.

In addition, the functionality of the α-onocerin pathway proteins fused to the fluorescent tags was tested. No α-onocerin was detected when the fusion constructs of OsONS1 were expressed alone in *N. benthamiana* leaves (Fig. 6, C and D), suggesting a detrimental effect of the tag on the enzymatic activity of OsONS1. However, when tagged OsONS1 was coexpressed with OsSQE1 or OsSQE2 tagged with mRFP1 at the C terminus, α-onocerin was detected, with no significant differences in α-onocerin levels between the different combinations. These results indicated that tagged OsONS1 could still produce α-onocerin but required higher abundance of SDO.

A significant fluorescence lifetime decrease was observed for the donor OsONS1-eGFP in the presence of OsSQE1-mRFP1 as compared with that of OsONS1-eGFP expressed alone, indicating protein-protein interaction between OsONS1 and OsSQE1 (Fig. 6A). A further significant decrease was observed when OsONS1-eGFP was expressed in the presence of OsSQE2-mRFP1. As negative controls, OsONS1-eGFP was coexpressed with either the soluble mRFP1 or SbCYP98A1-mRFP1. The latter cytochrome P450 enzyme from *Sorghum bicolor* is unrelated to the triterpenoid pathway but also localizes to the ER membrane. Neither of these controls showed a reduction of fluorescence lifetime for OsONS1-eGFP (Fig. 6A), demonstrating that the interactions observed for OsONS1 with OsSQE1 and OsSQE2 are specific.

o investigate whether the tag position influenced the protein-protein interaction, OsONS1 was N-terminally tagged to eGFP and coexpressed in *N. benthamiana* with C-terminally tagged OsSQEs. FLIM results showed that eGFP-OsONS1 fluorescence lifetime was not reduced when coexpressed with the negative controls, but a significant decrease of the fluorescence lifetime values was measured in the presence of OsSQE1-mRFP1, and an even further significant decrease was observed when coexpressed with OsSQE2-mRFP1 (Fig. 6B).

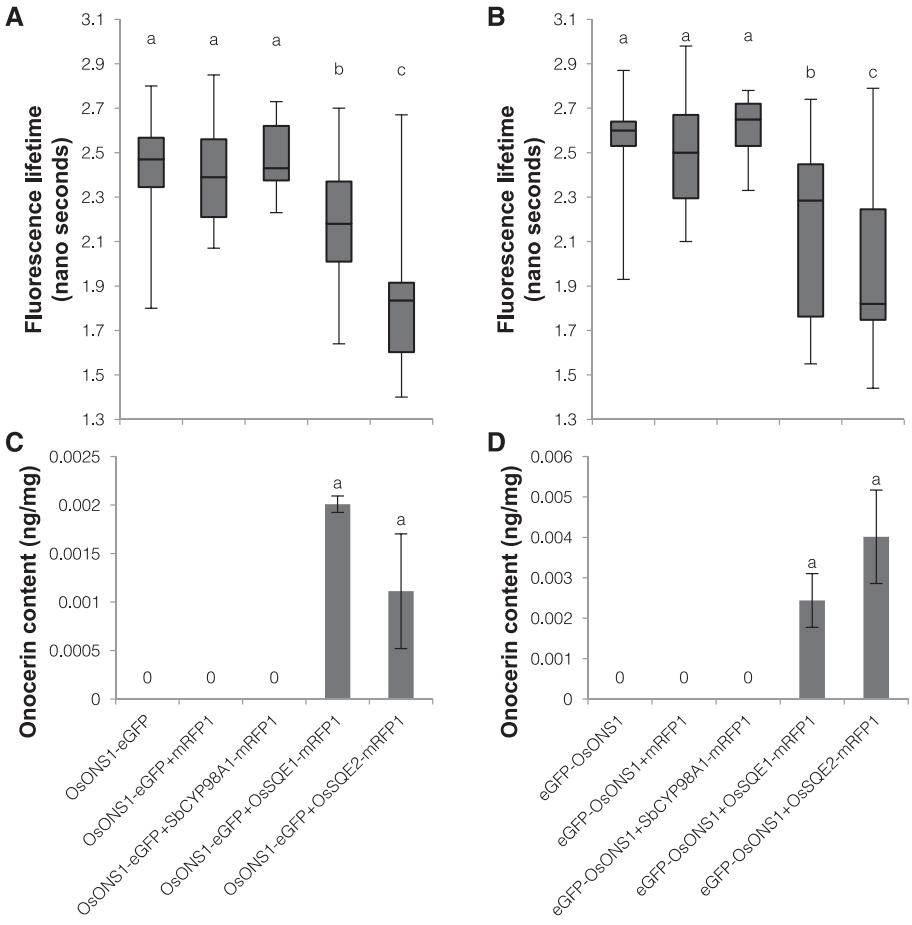

Figure 6. OsONS1 interacts with both OsSQE1 and OsSQE2. A, FLIM values for *OsONS1* tagged with *eGFP* on the C terminus coexpressed with several *mRFP1*-fused constructs in transiently transformed *N. benthamiana* leaves. B, FLIM values for *OsONS1* tagged with *eGFP* on the N terminus coexpressed with several *mRFP1*-tagged constructs in transiently transformed *N. benthamiana* leaves. C, α-Onocerin content of *N. benthamiana* leaves transiently transformed with *OsONS1-eGFP* coexpressed with several *mRFP1*-tagged constructs. D, α-Onocerin content of *N. benthamiana* leaves transiently transformed with *eGFP-OsONS1* coexpressed with several *mRFP1*-tagged constructs. For A and B, letters indicate significant differences determined by ANOVA/posthoc Scheffe's method at $P < 0.05$. For C and D, values represent means ± SE from three biological replicates; letters indicate significant differences determined by ANOVA/posthoc Tukey's HSD test at $P < 0.05$.

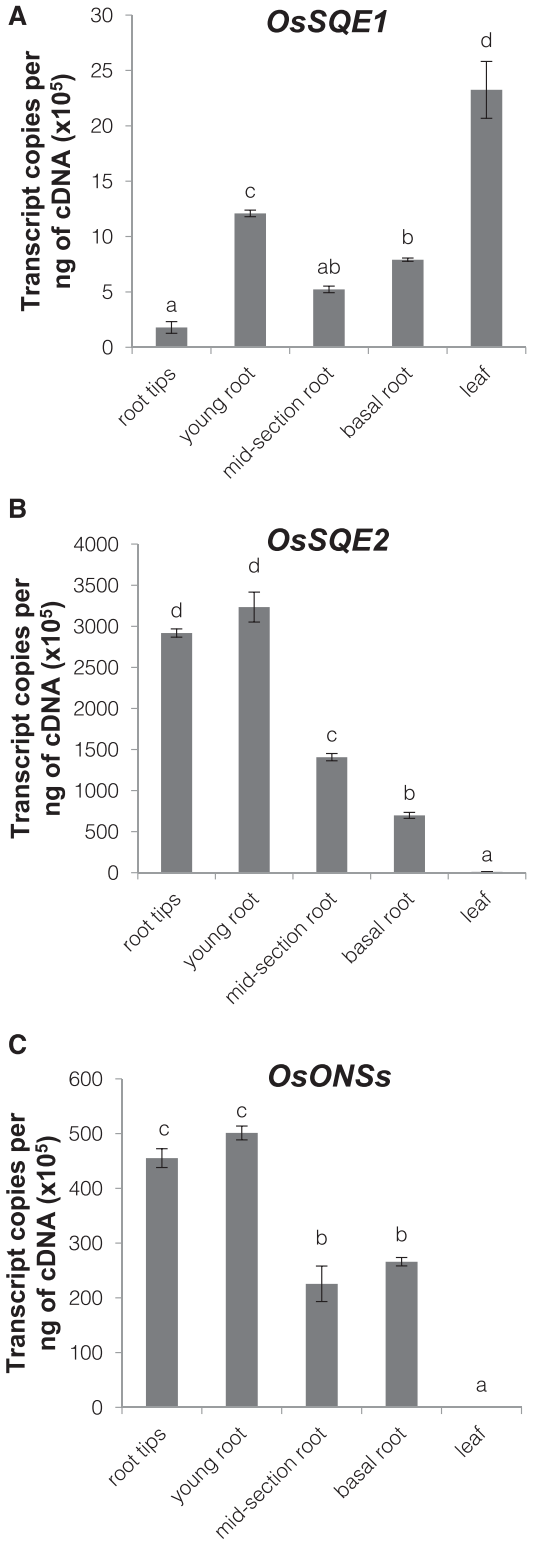

Figure 7. *OsSQE2* and *OsONSs* coexpress across root sections and leaves of *O. spinosa*. A, Absolute quantification of *OsSQE1* transcripts in different tissues of *O. spinosa*. B, Absolute quantification of *OsSQE2* transcripts in different tissues of *O. spinosa*. C, Absolute quantification of *OsONS* transcripts in different tissues of *O. spinosa*. qRT-PCR was performed on RNA extracted from the pooled tissues of five plants. Values represent means ± SE from three different poolings per tissue; letters indicate significant differences determined by ANOVA/posthoc Tukey's HSD test at $P < 0.05$.

OsONS1 and OsONS2 Coexpress with OsSQE2 in *O. spinosa* Root Sections

The reduced fluorescence lifetime observed for tagged OsONS1 in the presence of OsSQE2-mRFP1 as compared with that of OsSQE1-mRFP1 in the FLIM experiments is not enough to determine that OsSQE2 had a stronger protein-protein interaction or was the preferred partner of OsONS1. The lower fluorescence lifetime values could be due to the final positioning of fluorescent labels on the proteins with no actual biological significance. In addition, the fact that higher amounts of α-onocerin were detected when OsONS1 was coexpressed with OsSQE1 in *N. benthamiana* leaves raises the question of whether OsONS1 has a specific partner or whether it readily interacts with both OsSQE1 and OsSQE2. Therefore, the expression of *OsONSs*, *OsSQE1*, and *OsSQE2* was assessed by quantitative reverse transcription (qRT)-PCR in *O. spinosa* root sections and leaf tissues to determine possible coexpression. This analysis showed that the transcript copies of *OsSQE1* were generally 3 orders of magnitude lower than those of *OsSQE2* in root sections, except in the leaves, where *OsSQE1* transcript copies were 2-fold higher than those of *OsSQE2* (Fig. 7). Transcript copies of *OsSQE2* decreased from young root to midsection root and decreased further in the basal root. Transcript copies of *OsSQE2* dropped 72-fold in leaf tissue as compared with basal root tissues (Fig. 7B).

A specific primer pair could not be designed to discriminate between *OsONS1* and *OsONS2*; therefore, primers were designed in a conserved region to quantify both transcripts simultaneously. The *OsONSs* showed a similar transcript abundance pattern to that of *OsSQE2* across *O. spinosa* root sections. High transcript counts of *OsONSs* were detected in root tips and young roots; subsequently, transcript copies of *OsONS*s dropped from young roots by approximately half in midsection roots and basal roots, finalizing with an ~1,400-fold drop from basal root sections to leaf tissue. These data supported that *OsSQE2* may be the specific SQE for α-onocerin biosynthesis and is regulated at the transcriptional level, despite that coexpression in *N. benthamiana* showed that OsSQE1 can boost α-onocerin production of OsONS1 to higher levels than OsSQE2.

DISCUSSION

α-Onocerin Biosynthesis Differs in *O. spinosa* and *L. clavatum* and Is a Result of Convergent Evolution

Previously, it was shown that α-onocerin production in *L. clavatum* proceeds in two cyclization steps (Araki et al., 2016). LcLCC accepts SDO as a substrate and

initiates the cyclization cascade from one end of SDO to produce the bicyclic pre-α-onocerin (Fig. 4C), which, in turn, is cyclized by LcLCD from the remaining epoxide ring to α-onocerin. Here, we show that, in *O. spinosa*, a single OSC is capable of producing α-onocerin, in contrast to the previously described two-enzyme system of *L. clavatum*.

The biochemistry and the position of the α-onocerin synthases on the phylogenetic tree strongly indicate that the α-onocerin pathways in these two species evolved convergently. OsONS1 and OsONS2 group with highly specific lupeol synthases of other legumes, such as *L. japonicus* and *G. glabra* (Hayashi et al., 2004; Sawai et al., 2006). The *Ononis* and *Glycyrrhiza* genera belong to the monophyletic inverted repeat-lacking clade in the Fabaceae family (Wojciechowski et al., 2004), which is predicted to have originated before the Trifolieae clade, to which the *Ononis* genus belongs. This suggests that an OSC with a predisposition for lupeol production could have existed in the common ancestor of the *Ononis* genus and that this OSC could have undergone neofunctionalization to be able to produce α-onocerin.

As for the functional mechanism of α-onocerin production by OsONS1, neither multiple sequence alignments of deduced amino acid sequences of OsONSs and characterized OSCs nor the homology model of OsONS1 show indications of two catalytic motifs (DCTA) facing each other in the active site for simultaneous cyclization of SDO from both ends. This renders it more likely that OsONS1 is a multifunctional enzyme that is able to accept both SDO and pre-α-onocerin and perform the cyclization steps of both LcLCC and LcLCD. Indeed, the multiple sequence alignment of deduced amino acid sequences suggests that the synthesis of pre-α-onocerin by OsONS1 is possible, as the OsONS residue Leu-725 corresponds to that of yeast lanosterol synthase (Erg7) Phe-699 (Supplemental Fig. S3). This amino acid is predicted to stabilize the anti-Markovnikov secondary cation for C-ring expansion (Thoma et al., 2004), and changes influencing the position of this amino acid in the catalytic cavity have been reported to give bicyclic products. Since Leu is smaller than Phe, this change would enlarge the catalytic cavity and, most likely, result in destabilization of the anti-Markovnikov secondary cation, thereby disabling C-ring formation. In addition, the literature supports the possibility of OsONS1 being able to perform both cyclization steps. Previous communications reported that lanosterol synthase from rabbit could produce the tetracyclic compound **2** from the semicyclic compound **1** (Fig. 4D), thus providing proof that a full-pocket fit is not indispensable for OSC activity, as long as the epoxide required for initiation of the cyclization cascade is present (Van Tamelen et al., 1982). Possibly, the substrate specificity of the *L. clavatum* α-onocerin synthases could rely on amino acids in the OSC substrate channel. In fact, α-onocerin synthases of *O. spinosa* differ from those in *L. clavatum* in amino acids that correspond to residues described in the OSC substrate channel, in particular HsLAS Cys-233 and Ile-524, which are both involved in the passage of the substrate to the active site (Thoma et al., 2004), His-289 is involved in the hydrogen bond network of the channel constriction loop (Oliaro-Bosso et al., 2005), and Tyr-237 has been proposed to allow access of the substrate to the catalytic cavity by rotating (Oliaro-Bosso et al., 2011). Lycopods arose early on in the plant phylogeny; hence, LcLCC and LcLCD have perhaps had more time for substrate specialization. Conversely, it can be inferred that α-onocerin biosynthesis appeared more recently in the *Ononis* genus, since OsONSs stem from the highly specific lupeol synthase branch of OSCs. The appearance of two distinct α-onocerin synthases could relate to this substrate specialization happening in *O. spinosa*. Future work on site-directed mutagenesis of the above-mentioned residues and in vitro studies would provide insights into the specificity of α-onocerin synthases and in OSCs in general.

OsSQE1 and OsSQE2 Interact Specifically with OsONS1 and Boost α-Onocerin Production

Previously, Rowan et al. (1971) established that α-onocerin was produced exclusively from SDO by protein extracts of *O. spinosa* roots. Endogenous SQEs from *N. benthamiana* only provide enough SDO for OsONS1 to produce low amounts of α-onocerin in the transient transformation platform. In this study, we report that two SQEs from *O. spinosa* significantly boost α-onocerin production to different levels in *N. benthamiana* and that both show protein-protein interactions with OsONS1. The difference in their expression patterns suggests that one of the *OsSQEs* of *O. spinosa* may have specialized for the α-onocerin pathway.

The production of SDO appears to be a common feature of SQEs. The lack of substrate specificity of SQEs was demonstrated previously by Van Tamelen and Heys (1975), while Corey and Russey (1966) showed that SQE from rat microsomes can epoxidize both ends of squalene. Since then, several SQEs from different mammalian and plant sources have been shown to synthesize SDO in vitro (Bai et al., 1992; Nagumo et al., 1995; Rasbery et al., 2007). However, for these epoxidases to generate SDO, SQO must be allowed to accumulate for several hours by inhibiting the activity of OSCs (with AMO-1618 or DMAE-DHA; Field and Holmlund, 1977; Nagumo et al., 1995), suggesting that the rate of SDO production for OsSQEs is different from those reported for the previous SQEs.

In addition, the in planta role of SDO is not known, and it has not been isolated under normal physiological conditions but only when the catalytic activity of OSCs was inhibited, which leads to an overaccumulation of SQO that then can be epoxidized to SDO (Field and Holmlund, 1977; Nagumo et al., 1995). Nonetheless, 24,25-expoxycycloartenol has been reported to occur naturally in tobacco (*Nicotiana tabacum*) tissue cultures

(Schaefer et al., 1970), and this compound is likely to derive from the cyclization of SDO by cycloartenol synthase. In human cell cultures, some oxysterols have been shown to inhibit 3-hydroxy-3-methylglutaryl-coenzyme A reductase, suggesting that they have a regulatory role in sterol biosynthesis (Kandutsch et al., 1978; Spencer, 1994). In the *N. benthamiana* transient expression experiments, α-onocerin production by OsONS1 was 2.6-fold higher when coexpressed with OsSQE1 than with OsSQE2, in spite of OsSQE2 showing a stronger protein-protein interaction with OsONS1 (Fig. 6, A and B). These results suggest that the boost in α-onocerin production by *OsONSs* heterologously coexpressed with *OsSQEs* is most likely due to a higher SDO production by the OsSQEs than by the endogenous *N. benthamiana* SQEs. The protein-protein interactions of OsSQEs with OsONS1 would favor channeling of the SDO to α-onocerin production instead of oxysterols that might halt triterpenoid biosynthesis. In yeast, disruption of the C-4 demethylation complex of Erg25p/Erg26p/Erg27p/Erg28p in *erg*28 mutants reduces ergosterol levels compared with wild-type strains (Gachotte et al., 2001), demonstrating the existence of protein complexes in triterpenoid biosynthesis (Mo et al., 2002) and the importance of protein-protein interactions for metabolic flux in triterpenoid pathways. However, protein-protein interactions among enzymes in the early steps of triterpenoid biosynthesis had not been determined before, in spite of existing indirect evidence such as the C-terminal domain of Arabidopsis squalene synthase being required for efficient channeling of squalene to SQE (Kribii et al., 1997). The results shown here may pave the way for future investigations on the importance of SQEs and their interactions with OSCs in the production of specialized metabolites.

The Biosynthesis and Accumulation of α-Onocerin Differ across Root Sections

The FLIM experiments showed OsONS1 to have stronger protein-protein interactions with OsSQE2 than with OsSQE1 (Fig. 6, A and B). In accordance, *OsONSs* and *OsSQE2* coexpressed across root sections, suggesting that OsSQE2 may be the specific partner of OsONS1 in the α-onocerin pathway. In addition, the FLIM and qRT-PCR data suggest that the root tips and young root sections are the locations with highest α-onocerin biosynthetic activity. However, α-onocerin accumulation in the root sections contrasts with the expression patterns observed for the *OsONSs* and *OsSQE2*. While the basal and midsection roots show highest α-onocerin contents, they have lower transcript counts for *OsSQE2* and *OsONSs* compared with the root tips and young roots, in which no or only trace amounts of α-onocerin are observed, respectively.

In agreement with *OsSQE2* being the specific partner of *OsONS1*, it was concluded that *MtSQE2* was the specific SQE for saponin metabolism in *M. truncatula*, since it showed coexpression with *β-amyrin synthase* after root cultures were treated with methyl jasmonate (Suzuki et al., 2002). In the same study, *MtSQE1* was found to be lowly expressed in all tissues before or after methyl jasmonate induction. Similarly, in this study, a lower transcript copy number of *OsSQE1* compared with *OsSQE2* is reported in all root sections of *O. spinosa*.

Concerning the distribution of α-onocerin across the roots, analogous spatial-specific accumulation of triterpenoids has been observed in other plants as well. For example, a similar trend was observed for in vitro roots of *Peritassa laevigata*, where the accumulation of maytenin and 22β-hydroxy-maytenin in the mature root tissue decreased toward the root cap (Pina et al., 2016). However, no gene expression was measured in that study to allow comparing the regulation of biosynthetic genes with that in our study. The discrepancy of the conjecture of α-onocerin biosynthesis occurring primarily in root tips, but the product accumulating in the basal root, can be explained by an active transport of α-onocerin or the absence of special α-onocerin-storing structures in young roots as opposed to mature root sections. The spatial-specific distribution of α-onocerin in *O. spinosa* suggests that this compound may have a specific function in the plant, and our results will contribute to the unraveling of the biological function of α-onocerin in *O. spinosa*.

CONCLUSION

In this article, we characterized two OSCs from *O. spinosa* that are capable of producing α-onocerin when expressed individually in *N. benthamiana* leaves. The expression of *OsONS1* in the yeast strain GIL77 and phylogenetic analysis indicate that the *O. spinosa* α-onocerin synthases arose from a different evolutionary route from those of *L. clavatum*, meaning that the emergence of the α-onocerin pathways in these two species is the result of convergent evolution. In addition, two SQEs of *O. spinosa* specialized for α-onocerin production have been identified and characterized. Both OsSQE1 and OsSQE2 displayed protein-protein interactions with OsONS1 and boosted the α-onocerin production of OsONS1 by providing more SDO. The results described here will hopefully foster systematic studies on the convergent evolution of specialized metabolite pathways in unrelated plant species, a puzzling event, especially for compounds like α-onocerin, for which a specific biological target or function has not been assigned yet.

MATERIALS AND METHODS

Plant Material

Seeds of wild *Ononis spinosa* accessions were collected from different locations on the island of Zealand, Denmark, or procured from botanical gardens through the Botanic Gardens Conservation International Web site (https://www.bgci.org/). Commercially available seeds were purchased, and details on the origins and labels used throughout this experiment are given in Table I. The seeds were first nicked using a scalpel, then soaked in water for

48 h, and subsequently transferred to petri dishes that had a wet circular filter paper (Frisenette no. 118) for them to germinate. After 5 d, seedlings were transferred to either soil (Pindstrup substrate no. 2) or hydroponic solution [KH_2PO_4 0.2 mM, K_2SO_4 0.2 mM, $MgSO_40•7H_2O$ 0.3 mM, NaCl 0.1 mM, $Mg(NO_3)_20•6H_2O$ 0.3 mM, $Ca(NO_3)_20•4H_2O$ 0.9 mM, KNO_3 0.6 mM, and micronutrients Fe(III)-EDTA-Na 0.05 mM, $MnCl_20•4H_2O$ 7 μM, $ZnCl_2$ 0.7 μM, $CuSO_40•5H_2O$ 0.8 μM, H_3BO_3 2 μM, and $Na_2MoO_40•2H_2O$ 0.8 μM]; finally, this solution was adjusted to pH 5.5. Plants were grown in the greenhouse with conditions of 16-h day at 18°C and 8-h night at 15°C.

Generation of Hairy Root Lines

Seeds of OsDK7 were washed for 20 min in water with soap and sterilized in 0.5% (v/v) bleach for 20 min. After rinsing with sterile water three times, the sterilized seeds were plated on Murashige and Skoog (MS) medium. For hairy root induction, *Agrobacterium rhizogenes* strains LBA9402, R1200, and Arqua1 were transformed with the modified pJCV51 vector (https://gateway.psb.ugent.be) containing mRFP and a USER cloning cassette (New England Biolabs) and selected with spectinomycin resistance. A stripe of a bacterial colony was scraped off with a sterile scalpel blade and resuspended in 20 mL of PS buffer (10 mM PIPES [P8203; Sigma-Aldrich]/KOH, pH 6.8, and 200 mM sorbitol). The scalpel was dipped in the suspension and used to make incisions through the leaves, roots, hypocotyl, and cotyledons of in vitro cultured *O. spinosa*. Incised tissues were placed onto solid MS medium without antibiotics. After growing in the dark for 2 d, the inoculated tissues were transferred to fresh MS medium supplemented with 500 μg mL^{-1} cefotaxime, 250 μg mL^{-1} carbenicillin, and 50 μg mL^{-1} kanamycin. Then, the inoculated leaves were placed back in the dark and were regularly replaced in fresh medium containing all antibiotics. After 1 month, expanding tissues were tested for mRFP fluorescence.

Hairy root lines were imaged using a Leica M205FA fluorescence stereomicroscope equipped with a PLAN-APO 1.0× lens (Leica-10450028) and a Leica DFC450C camera. Images were acquired in the LAS 4.0 software (Leica), and scale bars were added using ImageJ software (Schneider et al., 2012).

Transcriptome Analysis and RACE on OSC Fragments

The wild accession OsDK7 was grown in hydroponics, and at 45 d after germination, the roots were cut in sections: root tips (1.5 cm from the tip), young root (5 cm after root tips), midsection root (half of the remainder root length), and basal root (remaining root base); tissues were frozen in liquid N_2 and processed immediately. The RNA was isolated from 100 mg of root section tissue using the Spectrum Plant Total RNA kit (Sigma-Aldrich) and digested with RNase-free DNase I (catalog no. 79254; Qiagen). The root tips of five plants were pooled to have enough tissue for RNA isolation. The quality and quantity of RNA were assayed using the Bioanalyzer 2100 (Agilent). Only RNA from root tips and midsection roots were shipped to Macrogen sequencing services for sequencing with the MiSeq Illumina platform to create paired-end read libraries. Total reads obtained for root tips and midsection roots amounted to 19.68 and 17 million, respectively. The quality of data sets was assayed with FastQC, reads containing an overall quality score below 20 were filtered out using the fastx toolkit, and low-quality bases were trimmed from the ends of the reads using Trimmomatic. To assemble a transcriptome representative of the whole root, the left-end files from root tips and midsection roots were merged, and the same was done for right-end sequence files. The merged files were matched with the paired_sequence_match.py script of paired_sequence_utils 0.1. A total of 16 million reads were input into the Trinity assembler (Grabherr et al., 2011) to obtain the de novo assembly of the *O. spinosa* root transcriptome. BLAST was downloaded from National Center for Biotechnology Information and used to BLAST the transcriptome locally against a small data set of sequences from previously characterized OSCs and SQEs retrieved from GenBank.

First-strand cDNA was synthesized from total RNA of roots from OsDK7 using the SuperScript III first-strand synthesis system (Thermo Fisher Scientific). Fragments of OSC were obtained by nested PCR with the degenerate primers 161S, 711A, 463S, and 603A (Supplemental Table S1) following the conditions reported by Kushiro et al. (1998). PCR fragments were separated by gel electrophoresis, and the band of ~450 bp was excised and ligated to the pJET1.2 cloning vector (catalog no. K1232; Thermo Fisher Scientific) following the manufacturer's instructions.

We used the SMARTer cDNA synthesis kit (Clontech) to generate 5′ RACE-ready first-strand cDNA and 3′ RACE-ready first-strand cDNA, from total RNA of OsDK7 roots, following the manufacturer's instructions. To obtain the 3′ end of OsONS1/OsONS2, OsSQE1, and OsSQE2, the 3′ template was amplified separately with primers RACE-ONS-F2, RACE-SQE1-F, and RACE-SQE2-F, respectively, using the Universal Primer Mix as indicated by the manufacturer. To obtain their 5′ ends, the 5′ template was amplified separately using RACE-ONS-R3, RACE-SQE1-R, RACE-SQE2-R2 (Supplemental Table S1), and the Universal Primer Mix. PCR conditions for all reactions were an initial denaturation of 95°C for 3 min, then 25 cycles of 95°C for 30 s, 65°C for 30 s, and 72°C for 3 min, and ended with a final extension of 72°C for 5 min, using the Advantage 2 polymerase mix provided. After gel electrophoresis, the bands from each reaction were blunted and ligated to the pJET1.2 cloning vector and transformed into *Escherichia coli* cells (E. cloni; Lucigen), then several clones of each fragment were cultured and subsequently sequenced. The 3′ and 5′ sequenced fragments of *OsONS1*, *OsONS2*, *OsSQE1*, and *OsSQE2* were aligned using the CLC main work bench version 7 (Qiagen) and were analyzed for the identification of single-nucleotide polymorphisms.

Phylogenetic Analysis and Homology Modeling

Sequences of OSCs used for phylogenetic analysis had the following GenBank accession numbers: KY625496 (OsONS1), KY625497 (OsONS2), KY657236 (OsBAS), KY657238 (OsCAS), KY657237 (OsLAS), D89619 (PsCASPEA), AB034802 (PsOSCPSY), AB034803 (PsOSCPSM), AJ430607 (MtBAS1), NM_106546 (AtLUP1), NM_106545 (AtLUP2), NM_106497 (AtPEN6), NM_123624 (AtMRN1), NM_106544 (AtBAS), NM_126681 (AtCAS1), AB247155 (AtLAS1), AB265170 (PgPNA), LC053637 (LcLCA), LC053635 (LcLCC), LC053636 (LcLCD), BAA86930 (OeOEW), AB116228 (GgLUS1), AB181245 (LjOSC3), AB244671 (LjOSC7), and AB116238 (CpCPQ).

Sequences of SQEs used for phylogenetic analysis had the following GenBank accession numbers: KY625494 (OsSQE1), KY625495 (OsSQE2), AJ430609 (MtSQE1), AJ430608 (MtSQE2), NM_104624 (AtSQE1), NM_127848 (AtSQE2), NM_119938 (AtSQE3), and XM_001781268 (PpSQE).

Protein-coding sequences were deduced using the Expasy translate tool (http://web.expasy.org/translate/). The evolutionary histories for the SQE and OSC protein sequences were inferred separately by using the maximum-likelihood method based on the JTT matrix-based model (Jones et al., 1992). The tree with the highest log likelihood was selected (−3,976.2379 for the SQE tree and −19,047.1377 for the OSC tree). Initial trees for the heuristic search were obtained by applying the neighbor-joining method to a matrix of pairwise distances estimated using a JTT model. The trees are drawn to scale, with branch lengths measured in the number of substitutions per site. The analysis involved eight and 24 amino acid sequences for the SQE and OSC trees, respectively. All positions containing gaps and missing data were eliminated. In total, there were 496 and 730 positions in the final data sets for the SQE and OSC trees, respectively. The statistical significance of each node was tested by the bootstrap method using 1,000 iterations. The evolutionary analyses were conducted in MEGA6 (Tamura et al., 2013). Multiple sequence alignments are given in Supplemental Figure S4.

For homology modeling, protein sequences of OsONS1 and HsLAS were aligned using MUSCLE, the alignment was uploaded to the Chimera GUI (Pettersen et al., 2004), and the modeler (Eswar et al., 2001) integrated tool was used to generate 10 models based on the HsLAS crystal structure (Protein Data Bank code 1w6k). The models were validated using Prosaweb (Wiederstein and Sippl, 2007), checked for Ramachandra outliers through the Molprobity server (Davis et al., 2007), and underwent manual inspection in Chimera itself. Chembio3D Ultra 14.0 (Perkin Elmer) was used to create the .mol2 files for pre-α-onocerin to use in Autodock 4 (Morris et al., 2009) for molecular docking simulations.

Multiple sequence alignments of OSC proteins for comparison of active residues was done with ClustalW, and residues were compared manually from available functional information on OSCs.

In Planta Transient Expression in *Nicotiana benthamiana* Leaves for Triterpenoid Analysis

The cDNA of *O. spinosa* roots was amplified by PCR using the attB-ONS primers for *OsONS1* and *OsONS2*, attB-SQE1 primers for *OsSQE1*, and attB-SQE2 primers for *OsSQE2* (Supplemental Table S1). Synthesis of the *LcLCC* and *LcLCD* genes was ordered from GeneArt Gene Synthesis (Invitrogen). The synthetic genes were amplified using attB-LCC and attB-LCD primers (Supplemental Table S1), and the amplicons were Gateway cloned into pDONR 207 (Invitrogen) and subsequently into the pEAQ-HT-DEST expression vector (Sainsbury and Lomonossoff, 2008). All PCR-based constructs were verified by

sequencing. Expression constructs were transformed into *Agrobacterium tumefaciens* strain AGL1. Colonies of *A. tumefaciens* were picked in the morning and precultured in 5 mL of Luria-Bertani medium with appropriate antibiotics. Afterward, 10 mL of Luria-Bertani medium containing antibiotics was inoculated with 50 μL of the preculture and incubated at 28°C overnight or until reaching an OD_{600} of 1.5. The cultures were centrifuged, the cell pellet was resuspended in infiltration buffer (10 mM $MgCl_2$, 10 mM MES, pH 5.6, and 100 μM acetosyringone), and OD_{600} was adjusted to 0.4. The suspension was incubated for 1 h on a shaker at 200 rpm at room temperature. Coinfiltration of agrobacteria was performed with cultures mixed in equal density. *N. benthamiana* plants were grown in soil (Pindstrup substrate no. 2) in a glasshouse with a 16-h day at 28°C and an 8-h night at 28°C. A transient expression assay was performed on 3-week-old plants, and leaves were harvested 5 d after infiltration, frozen in liquid N_2, and stored at −80°C for further processing.

TLC and GC-MS Analysis

α-Onocerin standard was crystallized from air-dried *O. spinosa* roots according to Berger and Sicker (2009). All tissues were crushed in N_2, and 100 mg of powder was extracted with 1 mL of dichloromethane for 1 h at 37°C shaking (450 rpm). For TLC analysis, 100 μL of this extract was concentrated by divided into aliquots to a glass vial insert and evaporated under vacuum for 20 min, subsequently redissolving in 20 μL of dichloromethane, and loaded on a TLC silica gel 60 F254 plate (catalog no. 105554; Merck). TLC plates were developed with 8:2 chloroform:ethyl acetate solution, and α-onocerin was visualized by staining with vanillin-phosphoric acid and heating to 115°C on a heating block.

For GC-MS analysis, 50 μL of extract was divided into aliquots into a glass insert containing 20 μL of internal standard (100 μM betulinic acid in methanol) and evaporated under vacuum. The glass inserts were sealed with airtight magnetic lids into GC-MS vials and derivatized by the addition of 30 μL of trimethylsilyl cyanide as described (Khakimov et al., 2013). All steps involving sample derivatization and injection were automated using a Multi-Purpose Sampler (MPS; Gerstel). After reagent addition, the sample was transferred into the agitator of the MPS and incubated at 40°C for 40 min at 750 rpm. Immediately after derivatization, 1 μL of the derivatized sample was injected in splitless mode. The spilt/splitless injector port was operated at 320°C. The septum purge flow and purge flow to split vent at 2.1 min after injection were set to 3 and 15 mL min^{-1}, respectively. The GC-MS system consisted of an Agilent 7890A GC device and an Agilent 5975C series MSD (Agilent Technologies). GC separation was performed on an Agilent HP-5MS column (30 m × 250 μm × 0.25 μm) by using hydrogen carrier gas at a constant flow rate of 1.2 mL min^{-1}. The GC oven temperature program was as follows: initial temperature, 40°C; equilibration time, 2 min; heat up to 270°C at the rate of 12°C min^{-1}; heat at the rate of 6°C min^{-1} until 310°C; and hold for 10 min. Mass spectra were recorded in the range of 50 to 700 mass-to-charge ratio with a scanning frequency of 2.2 scans s^{-1}, and the MS detector was switched off during the first 20 min of the run, since all targeted molecules eluted after this retention time. The transfer line, ion source, and quadrupole temperatures were set to 290°C, 230°C, and 150°C, respectively. The mass spectrometer was tuned according to the manufacturer's recommendation by using perfluorotributylamine. The MPS and GC-MS devices were controlled using vendor software Maestro (Gerstel).

Expression of OsONS1 in Yeast

The LR reaction was performed between pENTR207[OsONS1] vector (previously created for *N. benthamiana* transient transformation) and pESC-URA-tHMG1-DEST (Fiallos-Jurado et al., 2016) to obtain pESC-URA (GAL10/tHMG1; GAL1/OsONS1) plasmid for expression in yeast. The yeast strain GIL77 (gal2, hem3-6, erg7, ura3-167) was transformed with this plasmid and precultured at 30°C in synthetic defined medium containing Glc (Clontech) and the uracil dropout (-U) supplement (Clontech) and supplemented with 20 μg mL^{-1} ergosterol and 13 μg mL^{-1} hemin (all from Sigma-Aldrich). After 5 d, precultures were inoculated in the induction medium synthetic defined Gal/Raf-U containing 2% (w/v) Gal to a starting OD_{600} of 0.25 and incubated for 72 h. Cells from 1 mL of the culture were collected and lysed using equal volumes of 50% (v/v) ethanol and 40% (w/v) KOH according to Moses et al. (2014). The lysate was extracted twice using 500 μL of dichloromethane, and the organic phases were pooled, lyophilized to dryness, and derivatized using pyridine and *N*-methyl-*N*-(trimethylsilyl)trifluoroacetamide prior to GC-MS analysis.

Absolute Quantification by qRT-PCR

Gel electrophoresis confirmed that the primers designed for qRT-PCR (Supplemental Table S1) amplify only one amplicon. Amplicon sizes for *OsONSs*, *OsSQE1*, and *OsSQE2* are 290, 236, and 195 bp, respectively. The amplicons were excised and ligated into pJET1.2 vector. Plasmid concentrations were quantified with a nanodrop (ND-1000). The transcript copy per microliter of each fragment inside the pJET1.2 vector was calculated with the following equation (Whelan et al., 2003):

$$\text{Number of copies per } \mu\text{L} = \frac{6.022 \times 10^{23}(\text{copy/mol}) \times \text{DNA amount(g)}}{\text{DNA length (bp)} \times 660\ (\frac{\text{g}}{\text{mol·bp}})}$$

A 10-fold serial dilution series ranging from 1×10^6 to 1×10^{10} copies per 1 μL was prepared for each fragment, and to make the standard curves, Ct values were plotted against the log of the copy number.

Each tissue was analyzed in triplicate, synthesizing cDNA from 1 μg of total RNA using the SuperScript III kit, and final volume was adjusted to 10 ng μL^{-1}. All quantitative PCRs for the three primer sets were performed in the CFX384 real-time system (Bio-Rad) under the following conditions: 4 μL of PowerUp SYBR Green Master Mix (Thermo Fisher Scientific), 1 μL of forward primer (2 μM), 1 μL of reverse primer (2 μM), 1 μL of cDNA (10 ng μL^{-1}), and 1 μL of MilliQ water. The PCR conditions were initial 95°C for 5 min, followed by 40 cycles of 95°C for 15 s, 55°C for 15 s, and 72°C for 30 s.

Protein-Protein Interaction Monitored by FLIM

The preparation of mRFP1 and SbCYP98A1-mRFP1 constructs was as described (Laursen et al., 2016). The construction of *OsONS1*, *OsSQE1*, and *OsSQE2* C-terminally fused to eGFP or mRFP1 was done by amplifying the full-length coding sequences with appropriate primers (Supplemental Table S1), and the amplicons were inserted in the pCAMBIA1300/UeGFP or pCAMBIA1300/UmRFP1 vector, respectively, by the single-insert USER cloning technique (Geu-Flores et al., 2007). Finally, to create the *OsONS1* construct N-terminally fused to eGFP, the full-length coding sequence of *OsONS1* was amplified with appropriate primers and the amplicons were inserted into the pCAMBIA1300/eGFPU vector (Laursen et al., 2016) with USER cloning. For transient expression in *N. benthamiana*, constructs were transformed to *A. tumefaciens* LBA4404 *virGN54D* (van der Fits et al., 2000). Cultures were prepared as described above but adjusted to a final OD_{600} of 0.15. *A. tumefaciens* strains carrying the constructs of interest were coinfiltrated in equal densities with *A. tumefaciens* transformed with a pCAMBIA1300 vector for expression of the viral p19 silencing suppressor protein (Tzuri et al., 2015). Leaf discs from transformed plants were sampled 3 d after infiltration for observation by confocal laser scanning microscopy and FLIM. An SP5x confocal laser scanning microscopy device equipped with a DM6000 microscope (Leica) was used to record images of enzyme subcellular localization with settings described by Laursen et al. (2016). FLIM was performed by time-correlated single-photon counting using the Microtime 200 system (Picoquant), and measurements were done using an Olympus IX70 microscope with pulse laser excitation at 485 nm provided by a Picosecond Diode Laser (PDL 828 SepiaII; Picoquant) with settings as described (Laursen et al., 2016). Samples were scanned for 232 s with the accurate FLIM method on the SymPhoTime64 software (Picoquant). For each combination, measurements were calculated from at least 25 regions of interest from independent images and cells, with a threshold of 50 counted photons and a pixel binning of 2. Lifetime value populations were tested for statistical significance by one-way ANOVA/posthoc Scheffe's test using IBM SPSS Statistics 24 software.

Accession Numbers

GenBank accession numbers are as follows: KY625496 (OsONS1), KY625497 (OsONS2), KY657236 (OsBAS), KY657238 (OsCAS), KY657237 (OsLAS), KY625494 (OsSQE1), KY625495 (OsSQE2), D89619 (PsCASPEA), AB034802 (PsOSCPSY), AB034803 (PsOSCPSM), AJ430607 (MtBAS1), NM_106546 (AtLUP1), NM_106545 (AtLUP2), NM_106497 (AtPEN6), NM_123624 (AtMRN1), NM_106544 (AtBAS), NM_126681 (AtCAS1), AB247155 (AtLAS1), AB265170 (PgPNA), LC053637 (LcLCA), LC053635 (LcLCC), LC053636 (LcLCD), BAA86930 (OeOEW), AB116228 (GgLUS1), AB181245 (LjOSC3), AB244671 (LjOSC7), AB116238 (CpCPQ), AJ430609 (MtSQE1), AJ430608 (MtSQE2), NM_104624 (AtSQE1), NM_127848 (AtSQE2), NM_119938 (AtSQE3), and XM_001781268 (PpSQE).

Supplemental Data

The following supplemental materials are available.

Supplemental Figure S1. α-Onocerin accumulates in the roots of *O. spinosa* in a spatial-specific manner.

Supplemental Figure S2. Hairy root lines induced from *O. spinosa* produce α-onocerin with different levels of accumulation.

Supplemental Figure S3. Multiple sequence alignment shows that a conserved Phe residue of OSCs is substituted in α-onocerin synthases.

Supplemental Figure S4. Multiple sequence alignment of SQE and OSC deduced protein sequences.

Supplemental Table S1. Primer list.

ACKNOWLEDGMENTS

We thank Dr. Thure Pavlo Hauser for help in the collection and identification of wild *O. spinosa* accessions.

Received September 29, 2017; accepted November 29, 2017; published December 4, 2017.

LITERATURE CITED

Abe I (2014) The oxidosqualene cyclases: one substrate, diverse products. *In* Osbourn A, Goss RJ, Carter GT, eds, Natural Products. John Wiley & Sons pp. 295–316

Ageta H, Iwata K, Ootake Y (1962) Isolation of alpha-onocerin from Lycopodium clavatum Linn. Chem Pharm Bull (Tokyo) **10:** 637

Araki T, Saga Y, Marugami M, Otaka J, Araya H, Saito K, Yamazaki M, Suzuki H, Kushiro T (2016) Onocerin biosynthesis requires two highly dedicated triterpene cyclases in a fern Lycopodium clavatum. ChemBioChem **17:** 288–290

Athenstaedt K, Zweytick D, Jandrositz A, Kohlwein SD, Daum G (1999) Identification and characterization of major lipid particle proteins of the yeast Saccharomyces cerevisiae. J Bacteriol **181:** 6441–6448

Augustin JM, Kuzina V, Andersen SB, Bak S (2011) Molecular activities, biosynthesis and evolution of triterpenoid saponins. Phytochemistry **72:** 435–457

Bai M, Xiao XY, Prestwich GD (1992) Epoxidation of 2,3-oxidosqualene to 2,3;22,23-squalene dioxide by squalene epoxidase. Biochem Biophys Res Commun **185:** 323–329

Barton DHR, Overton KH (1955) Triterpenoids. Part XX. The constitution and stereochemistry of a novel tetracyclic triterpenoid. J Chem Soc (Resumed) 2639–2652

Benveniste P (2004) Biosynthesis and accumulation of sterols. Annu Rev Plant Biol **55:** 429–457

Berger S, Sicker D (2009) Classics in Spectroscopy: Isolation and Structure Elucidation of Natural Products. Wiley-VCH, Weinheim, Germany

Boar RB, Couchman LA, Jaques AJ, Perkins MJ (1984) Isolation from Pistacia resins of a bicyclic triterpenoid representing an apparent trapped intermediate of squalene 2,3-epoxide cyclization. J Am Chem Soc **106:** 2476–2477

Corey EJ, Russey WE (1966) Metabolic fate of 10,11-dihydrosqualene in sterol-producing rat liver homogenate. J Am Chem Soc **88:** 4751–4752

Davis IW, Leaver-Fay A, Chen VB, Block JN, Kapral GJ, Wang X, Murray LW, Arendall WB III, Snoeyink J, Richardson JS, et al (2007) MolProbity: all-atom contacts and structure validation for proteins and nucleic acids. Nucleic Acids Res **35:** W375–W383

Eswar N, Webb B, Marti-Renom MA, Madhusudhan MS, Eramian D, Shen MY, Pieper U, Sali A (2001) Comparative protein structure modeling using MODELLER. *In* Coligan JE, Dunn BM, Speicher DW, Wingfield PT, eds, Current Protocols in Protein Science. John Wiley & Sons, pp. 2.9.1–2.9.37

Fiallos-Jurado J, Pollier J, Moses T, Arendt P, Barriga-Medina N, Morillo E, Arahana V, de Lourdes Torres M, Goossens A, Leon-Reyes A (2016) Saponin determination, expression analysis and functional characterization of saponin biosynthetic genes in Chenopodium quinoa leaves. Plant Sci **250:** 188–197

Field RB, Holmlund CE (1977) Isolation of 2,3;22,23-dioxidosqualene and 24,25-oxidolanosterol from yeast. Arch Biochem Biophys **180:** 465–471

Gachotte D, Eckstein J, Barbuch R, Hughes T, Roberts C, Bard M (2001) A novel gene conserved from yeast to humans is involved in sterol biosynthesis. J Lipid Res **42:** 150–154

Geu-Flores F, Nour-Eldin HH, Nielsen MT, Halkier BA (2007) USER fusion: a rapid and efficient method for simultaneous fusion and cloning of multiple PCR products. Nucleic Acids Res **35:** e55

Grabherr MG, Haas BJ, Yassour M, Levin JZ, Thompson DA, Amit I, Adiconis X, Fan L, Raychowdhury R, Zeng Q, et al (2011) Full-length transcriptome assembly from RNA-Seq data without a reference genome. Nat Biotechnol **29:** 644–652

Hayashi H, Huang P, Takada S, Obinata M, Inoue K, Shibuya M, Ebizuka Y (2004) Differential expression of three oxidosqualene cyclase mRNAs in *Glycyrrhiza glabra*. Biol Pharm Bull **27:** 1086–1092

Hayes SP (2012) Studies into the occurrence of a-onocerin in restharrow. PhD thesis. University of Nottingham, Nottingham, UK

Hlasiwetz H (1855) Ueber die Wurzel der Ononis spinosa. J Prakt Chem **65:** 419–450

Jones DT, Taylor WR, Thornton JM (1992) The rapid generation of mutation data matrices from protein sequences. Comput Appl Biosci **8:** 275–282

Kandutsch AA, Chen HW, Heiniger HJ (1978) Biological activity of some oxygenated sterols. Science **201:** 498–501

Khakimov B, Motawia MS, Bak S, Engelsen SB (2013) The use of trimethylsilyl cyanide derivatization for robust and broad-spectrum high-throughput gas chromatography-mass spectrometry based metabolomics. Anal Bioanal Chem **405:** 9193–9205

Kribii R, Arró M, Del Arco A, González V, Balcells L, Delourme D, Ferrer A, Karst F, Boronat A (1997) Cloning and characterization of the Arabidopsis thaliana SQS1 gene encoding squalene synthase: involvement of the C-terminal region of the enzyme in the channeling of squalene through the sterol pathway. Eur J Biochem **249:** 61–69

Kushiro T, Shibuya M, Ebizuka Y (1998) β-Amyrin synthase: cloning of oxidosqualene cyclase that catalyzes the formation of the most popular triterpene among higher plants. Eur J Biochem **256:** 238–244

Lalonde S, Ehrhardt DW, Loqué D, Chen J, Rhee SY, Frommer WB (2008) Molecular and cellular approaches for the detection of protein-protein interactions: latest techniques and current limitations. Plant J **53:** 610–635

Laursen T, Borch J, Knudsen C, Bavishi K, Torta F, Martens HJ, Silvestro D, Hatzakis NS, Wenk MR, Dafforn TR, et al (2016) Characterization of a dynamic metabolon producing the defense compound dhurrin in sorghum. Science **354:** 890–893

Leber R, Landl K, Zinser E, Ahorn H, Spök A, Kohlwein SD, Turnowsky F, Daum G (1998) Dual localization of squalene epoxidase, Erg1p, in yeast reflects a relationship between the endoplasmic reticulum and lipid particles. Mol Biol Cell **9:** 375–386

Lodeiro S, Xiong Q, Wilson WK, Kolesnikova MD, Onak CS, Matsuda SPT (2007) An oxidosqualene cyclase makes numerous products by diverse mechanisms: a challenge to prevailing concepts of triterpene biosynthesis. J Am Chem Soc **129:** 11213–11222

Mo C, Valachovic M, Randall SK, Nickels JT, Bard M (2002) Protein-protein interactions among C-4 demethylation enzymes involved in yeast sterol biosynthesis. Proc Natl Acad Sci USA **99:** 9739–9744

Morris GM, Huey R, Lindstrom W, Sanner MF, Belew RK, Goodsell DS, Olson AJ (2009) AutoDock4 and AutoDockTools4: automated docking with selective receptor flexibility. J Comput Chem **30:** 2785–2791

Moses T, Pollier J, Almagro L, Buyst D, Van Montagu M, Pedreño MA, Martins JC, Thevelein JM, Goossens A (2014) Combinatorial biosynthesis of sapogenins and saponins in Saccharomyces cerevisiae using a C-16α hydroxylase from Bupleurum falcatum. Proc Natl Acad Sci USA **111:** 1634–1639

Nagumo A, Kamei T, Sakakibara J, Ono T (1995) Purification and characterization of recombinant squalene epoxidase. J Lipid Res **36:** 1489–1497

Oliaro-Bosso S, Caron G, Taramino S, Ermondi G, Viola F, Balliano G (2011) Characterization of the channel constriction allowing the access of the substrate to the active site of yeast oxidosqualene cyclase. PLoS ONE **6:** e22134

Oliaro-Bosso S, Schulz-Gasch T, Balliano G, Viola F (2005) Access of the substrate to the active site of yeast oxidosqualene cyclase: an inhibition and site-directed mutagenesis approach. ChemBioChem **6:** 2221–2228

Pettersen EF, Goddard TD, Huang CC, Couch GS, Greenblatt DM, Meng EC, Ferrin TE (2004) UCSF Chimera: a visualization system for exploratory research and analysis. J Comput Chem **25:** 1605–1612

Pina ES, Silva DB, Teixeira SP, Coppede JS, Furlan M, França SC, Lopes NP, Pereira AMS, Lopes AA (2016) Mevalonate-derived quinonemethide triterpenoid from in vitro roots of Peritassa laevigata and their localization in root tissue by MALDI imaging. Sci Rep **6:** 22627

Rasbery JM, Shan H, LeClair RJ, Norman M, Matsuda SPT, Bartel B (2007) Arabidopsis thaliana squalene epoxidase 1 is essential for root and seed development. J Biol Chem **282:** 17002–17013

Rowan MG, Dean PDG (1972) α-Onocerin and sterol content of twelve species of Ononis. Phytochemistry **11:** 3263–3265

Rowan MG, Dean PDG, Goodwin TW (1971) The enzymic conversion of squalene, 2(3),22(23)-diepoxide to α-onocerin by a cell-free extract of Ononis spinosa. FEBS Lett **12:** 229–232

Sainsbury F, Lomonossoff GP (2008) Extremely high-level and rapid transient protein production in plants without the use of viral replication. Plant Physiol **148:** 1212–1218

Sawai S, Shindo T, Sato S, Kaneko T, Tabata S, Ayabe SI, Aoki T (2006) Functional and structural analysis of genes encoding oxidosqualene cyclases of Lotus japonicus. Plant Sci **170:** 247–257

Schaefer PC, de Reinach F, Ourisson G (1970) The conversion of parkeol into its 24,25-epoxide by tissue cultures of Nicotiana tabacum. Eur J Biochem **14:** 284–288

Schneider CA, Rasband WS, Eliceiri KW (2012) NIH Image to ImageJ: 25 years of image analysis. Nat Methods **9:** 671–675

Spencer TA (1994) The squalene dioxide pathway of steroid biosynthesis. Acc Chem Res **27:** 83–90

Suzuki H, Achnine L, Xu R, Matsuda SPT, Dixon RA (2002) A genomics approach to the early stages of triterpene saponin biosynthesis in Medicago truncatula. Plant J **32:** 1033–1048

Tamura K, Stecher G, Peterson D, Filipski A, Kumar S (2013) MEGA6: Molecular Evolutionary Genetics Analysis version 6.0. Mol Biol Evol **30:** 2725–2729

Thoma R, Schulz-Gasch T, D'Arcy B, Benz J, Aebi J, Dehmlow H, Hennig M, Stihle M, Ruf A (2004) Insight into steroid scaffold formation from the structure of human oxidosqualene cyclase. Nature **432:** 118–122

Tian BX, Eriksson LA (2012) Catalytic mechanism and product specificity of oxidosqualene-lanosterol cyclase: a QM/MM study. J Phys Chem B **116:** 13857–13862

Turini FG, Bräuchler C, Heubl G (2010) Phylogenetic relationships and evolution of morphological characters in Ononis L. (Fabaceae). Taxon **59:** 1077–1090

Tzuri G, Zhou X, Chayut N, Yuan H, Portnoy V, Meir A, Sa'ar U, Fabian B, Mazourek M, Lewinsohn E, et al (2015) Correction. Plant J **83:** 940

van der Fits L, Deakin EA, Hoge JHC, Memelink J (2000) The ternary transformation system: constitutive virG on a compatible plasmid dramatically increases Agrobacterium-mediated plant transformation. Plant Mol Biol **43:** 495–502

Van Tamelen EE, Heys JR (1975) Enzymic epoxidation of squalene variants. J Am Chem Soc **97:** 1252–1253

Van Tamelen EE, Leopold EJ, Marson SA, Waespe HR (1982) Action of 2,3-oxidosqualene lanosterol cyclase on 15′-nor-18,19-dihydro-2,3-oxidosqualene. J Am Chem Soc **104:** 6479–6480

Whelan JA, Russell NB, Whelan MA (2003) A method for the absolute quantification of cDNA using real-time PCR. J Immunol Methods **278:** 261–269

Wiederstein M, Sippl MJ (2007) ProSA-web: interactive web service for the recognition of errors in three-dimensional structures of proteins. Nucleic Acids Res **35:** W407–W410

Wojciechowski MF, Lavin M, Sanderson MJ (2004) A phylogeny of legumes (Leguminosae) based on analysis of the plastid matK gene resolves many well-supported subclades within the family. Am J Bot **91:** 1846–1862

Wu TK, Wang TT, Chang CH, Liu YT, Shie WS (2008) Importance of Saccharomyces cerevisiae oxidosqualene-lanosterol cyclase tyrosine 707 residue for chair-boat bicyclic ring formation and deprotonation reactions. Org Lett **10:** 4959–4962

Xu R, Fazio GC, Matsuda SPT (2004) On the origins of triterpenoid skeletal diversity. Phytochemistry **65:** 261–291